International Journal of Heat and Mass Transfer 87 (2015) 11–23

Contents lists available at ScienceDirect

International Journal of Heat and Mass Transfer

journal homepage: www.elsevier.com/locate/ijhmt

Pushing the limits of vertical naturally-cooled heatsinks; Calculations and design methodology

Mehran Ahmadi, Mohammad F. Pakdaman, Majid Bahrami *

Laboratory for Alternative Energy Conversion (LAEC), School of Mechatronic Systems Engineering, Simon Fraser University (SFU), Surrey, BC, Canada

ARTICLE INFO

Article history:
Received 18 March 2015
Received in revised form 27 March 2015
Accepted 27 March 2015

Keywords:
Natural convection
Interrupted fins
Optimum fin arrangement
Analytical solution
Integral technique
Experimental study
Numerical simulation

ABSTRACT

Heatsinks are essential parts of any thermal management system. High performance heatsinks are required for the cooling systems to be able to manage the ever-increasing power density in electronics and power electronics. The focus of this paper is on the design of high performance naturally-cooled heatsinks with vertical rectangular interrupted fins. A systematic analytical approach is taken, to solve the governing equations of the air flow and heat transfer. Closed-form correlations are presented for temperature and velocity distribution, and an easy-to-use method is introduced to design such heatsinks. Numerical simulations are used to provide better understanding of the physics of flow and heat transfer mechanism. An extensive experimental study is also conducted to verify the results from analytical solution and numerical simulation. Results show that the new-designed heatsinks are capable of dissipating heat up to 5 times more than currently available naturally-cooled heatsinks, with up to 30% less weight. The new heatsinks can increase the capacity of passive thermal management systems significantly.

1. Introduction

Thermal management of electronics/power electronics has wide applications in different industries such as; telecommunication (datacenters and outdoor enclosures), automotive (conventional, hybrid, electric, and fuel cell vehicles), renewable energy systems (solar panels and wind turbine), etc. About 55% of failures in electronics during operation has thermal root [1]. The rate of failure due to overheating, nearly doubles with every 10 °C increase above the operating temperature [2]. Considering the ever-increasing desire to miniaturization in the industry, which leads to higher power densities, thermal management has become the limiting factor in the development of such devices, and reliable low-cost methods of cooling are more and more required. The importance of efficient thermal management systems is also reflected in the market. Thermal management technology market was valued at $10.1 billion in 2013 and reached $10.6 billion in 2014. Total market value is expected to reach $14.7 billion by 2019 [3]. Thermal management hardware, e.g. fans and heatsinks, accounts for about 84% of the total market. Other cooling product segments, e.g. software, thermal interface materials (TIM), and substrates, each account for 4–6% of the market [3].

Passive cooling is a widely preferred cooling method for electronic and power electronic devices. High reliability, no noise and no parasitic power make natural convection and other passive cooling methods attractive for sustainable and "green" systems. As an example, in telecom industry, integrating passive cooling techniques with conventional cooling strategies can reduce the energy required for thermal management from 28% of total energy consumption [4], to 15% in general [5] and 0% in some cases [6].

Considering an available temperature difference between the heat source and cooling medium, this thermal budget is always spent in the thermal resistances along the heat path. These thermal resistances, in most cases include: (i) thermal contact resistance at the solid–solid interface, (ii) spreading resistance, due to changes in geometry, (iii) bulk resistance, due to the materials' thermophysical properties, and (iv) film resistance existing at the solid–fluid interface due to thermal boundary layer. Except for the film resistance, the rest of above-mentioned thermal resistances are acting similarly between active and passive cooling systems. The effect of film resistance appears in the heatsink, and consequently design of high performance naturally-cooled heatsinks becomes very important in a fully passive thermal management system.

This paper provides an easy-to-use design method for a specific type of naturally-cooled heatsinks, namely interrupted fins. Naturally-cooled heatsinks with interrupted fins are shown to have very high performance compared to continuous fins, staggered

* Corresponding author. Tel.: +1 (778) 782 8587.
E-mail address: mbahrami@sfu.ca (M. Bahrami).

http://dx.doi.org/10.1016/j.ijheatmasstransfer.2015.03.086
0017-9310/

Nomenclature

General symbols

A	surface area, m^2
c_p	specific heat, J/kg K
g	gravitational acceleration, m/s^2
G	gap length, m
Gr	Grashof number, $g\beta\Delta Ts^3/v^2$
h	heat transfer coefficient, W/m^2 K
H	fin height, m
k	thermal conductivity, W/m K
l	fin length, m
L	baseplate length, m
m	number of fin rows
n	number of fin columns
Nu	Nusselt number, hs/k
P	heater power, W
Pr	Prandtl number, v/α
$\dot{q}$	heat flux, W/m^2
Q	total heat transfer, W
Ra	Rayleigh number, $g\beta\Delta Ts^3/v\alpha$
s	fin spacing, m
t	thickness, m
T	temperature, K
u	velocity in x-direction, m/s
v	velocity in y-direction, m/s
W	baseplate width, m
x	direction parallel to fins, m
y	direction normal to fins, m
z	direction normal to x and y in Cartesian coordinate

Greek symbols

α	thermal diffusivity, m^2/s
β	coefficient of volume expansion, K^{-1}
Δ	difference
ε	channel slenderness, l/s
ϕ	coefficient appears in gap velocity
φ	coefficient appears in gap velocity
ι	coefficient appears in gap temperature
μ	dynamic viscosity, kg/m s
v	kinematic viscosity, m^2/s
ϑ	constant appears in gap temperature
ρ	density, kg/m^3
σ	parameter appears in gap temperature, 1/m
ς	parameter appears in gap velocity, 1/m
ω_R	uncertainty
ξ	gap width, m

Subscripts

∞	ambient properties
C	channel
$C.V.$	control volume
G	gap
in	inlet of channel/gap
$N.C.$	natural convection
out	outlet of channel/gap
$Rad.$	radiation
$total$	total heat transfer
w	wall properties

interrupted fins, and even pin fins [7], and they currently exist in the market (Fig. 1a), mostly used for military applications that require high reliability, and high mechanical strength. Interruptions are discontinuities added fins to postpone the thermal boundary layer emergence in the channel flow between two adjacent walls (Fig. 1b); thus increase the total heat transfer rate [8]. Additionally, interruptions lead to considerable weight reduction, which in turn, can lower the manufacturing and material costs. It should be noted that interrupted fin arrangement is a more general form of geometry and includes both continuous and pin fins at the limit. Where the interruption length approaches zero or the fin length approached to the values close to fin thickness, continuous fin and pin fin geometries are respectively. In other words, continuous and pin fins are two extreme cases of the targeted interrupted fins. Fin interruption is common in industry and have been extensively studied for internal natural convection [9,10] and forced convection [11]. However, to the authors' best knowledge no comprehensive study is available for natural convection from interrupted fins. The present study aims to address this shortcoming.

1.1. Literature review

A general overview on pertinent literature in the area of natural convection heat transfer from fins is provided in this section. The focus of this study is on natural convection heat transfer from vertical rectangular interrupted fins.

1.1.1. Single wall

A variety of theoretical expressions, graphical correlations and empirical equations have been developed to calculate the coefficient of natural convection heat transfer from vertical plates. Ostrach [12] made an important contribution on analyzing the natural convection heat transfer from a vertical wall. He analytically solved laminar boundary layer equations using similarity methods for uniform fin temperature condition and developed a relationship for the Nusselt number for different values of Prandtl number. As well, Sparrow and Gregg [13] used similarity solutions for boundary layer equations for the cases of uniform surface heat flux. Merkin [14], also used similarity solution to solve natural convection heat transfer from a vertical plate with non-uniform wall temperature and wall heat flux. Churchill and Chu [15] developed an expression for Nusselt number for all ranges of the Rayleigh, and Pr numbers. Yovanovich and Jafarpur [16] studied the effect of orientation on natural convection heat transfer from finite plates. Cai and Zhang [17] found an explicit analytical solution for laminar natural convection in both heating and cooling boundary conditions.

1.1.2. Parallel plates

Finned surfaces are widely used for enhancement of heat transfer [18,19]. Natural convection heat transfer from vertical rectangular fins is a well-established subject in the literature. Pioneering analytical work in this area was carried out by Elenbaas [20]. He investigated isothermal finned heatsink semi-analytically and experimentally. His study resulted in general relation for average Nusselt number for vertical rectangular fins; which was not accurate for small values of fin spacing. Churchill [21] and Churchill and Chu [15] developed a general correlation for the average Nusselt number for vertical channels using the theoretical and experimental results reported by a number of

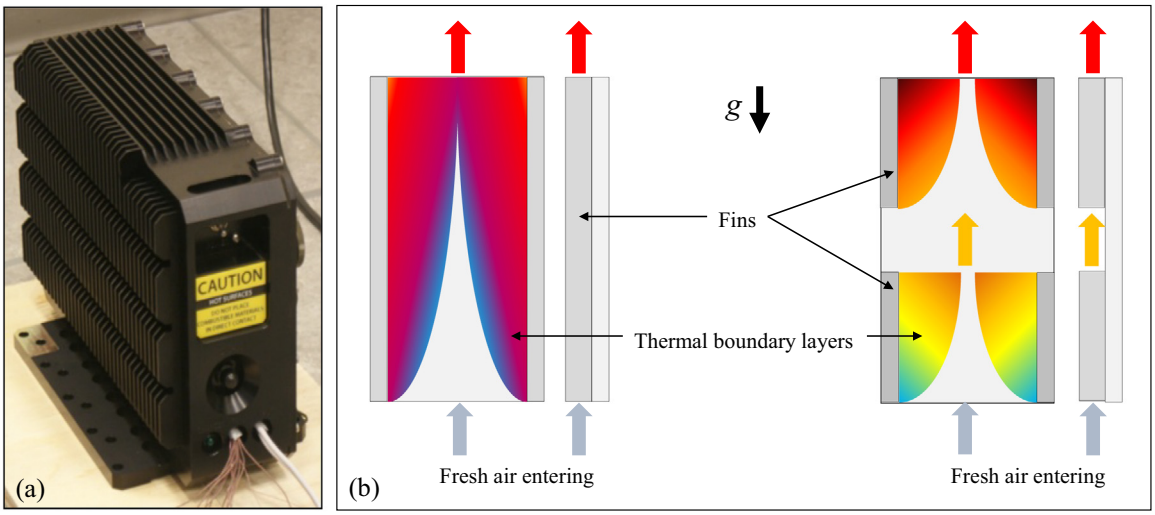

Fig. 1. (a) A sample of commercially available enclosure with interrupted fins, (b) effect of adding interruptions on thermal boundary layer and heat transfer.

authors. Bar-Cohen and Rohsenow [22] also performed a semi-analytical study to investigate the natural convection heat transfer from two vertical parallel plates. They developed a relationship for the average Nusselt number as a function of the Rayleigh number for isothermal and isoflux plates. Bodoia and Osterle [23] followed Elenbaas [20] and used a numerical approach to investigate the developing flow in a vertical and the natural convection heat transfer between symmetrically heated, isothermal plates in an effort to predict the channel length required to achieve fully developed flow as a function of the channel width and wall temperature. Ofi and Hetherington [24] used a finite element method to study natural convection heat transfer from open vertical channels. Culham et al. [25] also developed a numerical code to simulate free convective heat transfer from a vertical fin array. Several experimental studies were carried out on this topic. Sparrow and Acharya [26], Starner and McManus [27], Welling and Wooldridge [28], Edward [29], Chaddock [30], Aihara [31–34], Leung et al. [35–41], and Van de Pol and Tierney [42] are some examples. These studies were mostly focused on the effects of varying fin geometric parameters, the array, and baseplate orientation.

1.1.3. Interrupted fins

Effect of interruptions on forced convection is a mature subject in the literature. DeJong and Jacobi [43] did an extensive experimental study on different geometries of fin arrangement, including offset strip (staggered) fins and louvered fins. Brutz et al. [44] investigated the effect of unsteady forcing on forced convection heat transfer from interrupted fins. Jensen et al. [45] also performed a multi-objective thermal design optimization on different forced-air-cooled heatsinks, including continuous fin, pin fin, and interrupted fin with in-line and staggered arrangement. In case of natural convection heat transfer, Bejan et al. [46] used constructal method to optimize the distribution of discrete heat sources cooled by laminar natural convection. Sobel et al. [47] experimentally compared a staggered array of interrupted fins to continuous fins. They concluded that there is a significant increase in Nusselt number even beyond the meeting point of the boundary layers in the channel. However their results show that as the fin length increases, the relative advantage of the staggered arrangement decreases and the performance falls eventually below that of continuous fins. Sparrow and Prakash [48], numerically solved natural convection heat transfer from a staggered array of interrupted fins and compared the total heat transfer to continuous fins with the same surface area. They showed 100% enhancement for cases similar to pin fins, for a specific range of hydraulic diameter and Rayleigh number. Daloglu and Ayhan [9] investigated the effects of periodically installed fin arrays inside an open ended enclosure experimentally. They tested various arrangements and relatively large range of Rayleigh number, and showed the diverse effect of interrupted fins on internal natural convection heat transfer compared to continuous fins. Gorobets [49] performed and analytical study on natural convection heat transfer from staggered arrangement of fins and showed 50–70% enhancement compared to continuous fins. The few available studies on interrupted fins are mainly focused on staggered fin arrangement. Recently in an experimental and numerical study, we showed higher performance of interrupted fins compared to continuous fins [7,50]. However no detailed information, including velocity and temperature behavior, heat transfer calculation, fin design criteria, etc. is available for such fin type. To the best knowledge of author, no systematic study on interrupted vertical naturally-cooled fin arrays is currently available in the literature for the case of laminar natural convection heat transfer. As such, the goal of this study is to address this shortcoming in the literature and to investigate natural convection heat transfer from vertical rectangular interrupted fins, and develop a design tool to enable finding the optimum fin arrangement in such heatsinks.

2. Problem statement

The objective of this study is to develop an analytical model that can predict the natural convection heat transfer from a square array of vertical rectangular isothermal fins. Fig. 2 schematically shows the fins arrangement, parameters used to define the geometry, and control volumes used to model the heat transfer. To solve the problem, the domain is divided into multiple sub-domains, containing the channels made by two adjacent columns of fins, and the gaps region between two fin rows. The effects of neighboring channels on each other are neglected, so the problem is only solved between two fin columns and then the solution is extended to the whole domain. The problem is divided into two parts; (i) channel flow which contains the region between two neighboring fins, and (ii) gap flow which is related to the void region between two rows of fins. Each part is solved separately, and the solution of each part is superposed to solve the whole domain.

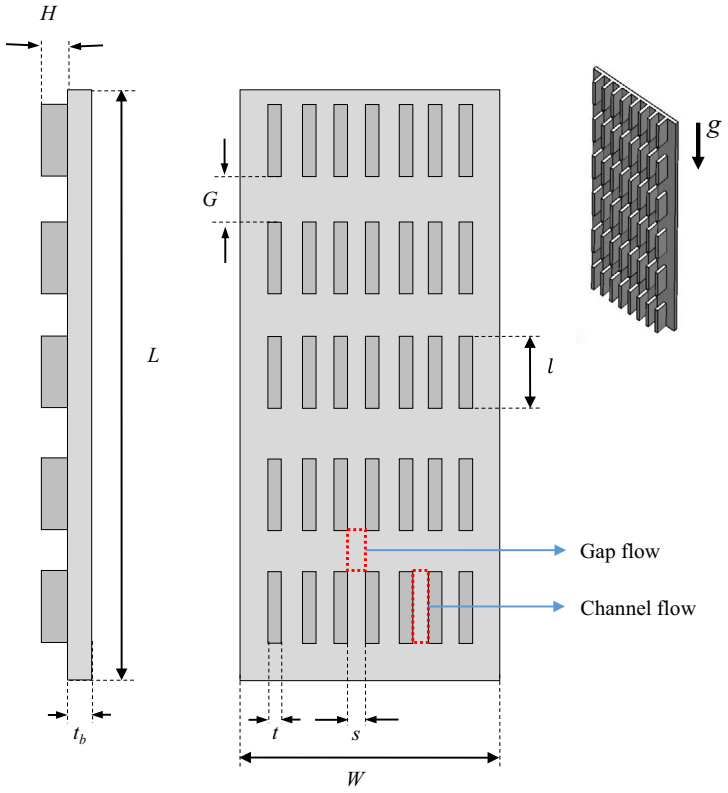

Fig. 2. A schematic of heatsink with interrupted fins, geometrical parameters used to address fin parameters, and the regions related to channel flow and gap flow.

3. Solution methodology

As shown in [7,8], adding interruption to a fin array will force the boundary layer to reset and increase the heat flux from the fins; however, cutting fins to add interruptions will result in losing surface area, which leads to a decrease in total heat transfer from the heatsink. In order to consider these two competing trends in our heatsink design, it is intended to find the optimum geometrical parameters, i.e. fin spacing, s, fin length, l, and gap length, G, to maximize the total heat transfer from an available area of base-plate by length of, L, and width of W. As explained briefly in Section 2, the problem is broken into a number of channels and gaps, stacked on top of each other. To solve for the whole domain, using the known boundary conditions at x-direction, the velocity and temperature profiles are obtained separately for the channels and the gaps, with outlet condition from the first channel considered as inlet condition to the first gap, and outlet condition from the first gap used as inlet condition to the second channel, and so on. After obtaining all the velocity and temperature profiles for the whole domain, the heat transfer from each channel is calculated and summed up to find the overall heat transfer from the heatsink.

3.1. Channel flow

The control volume considered for the channel flow is shown in Fig. 3. In [51], we used integral technique to find the velocity and temperature distribution in the channel made by two parallel isothermal walls. These equations can be rewritten in terms of channel average inlet velocity, as;

$$u_C(x,y) = -\frac{1}{4\nu}\left(g\beta\Delta T s^2 - (\beta g s^2\Delta T - 8\nu u_{in,C})e^{-\frac{5\nu\left(\beta g s^2\Delta T + 24\nu u_{in,C}\right)x}{s^2 u_{in,C}\left(\beta g s^2\Delta T - 8\nu u_{in,C}\right)}}\right)\left(\left(\frac{y}{s}\right)^2 - \frac{1}{4}\right) \tag{1}$$

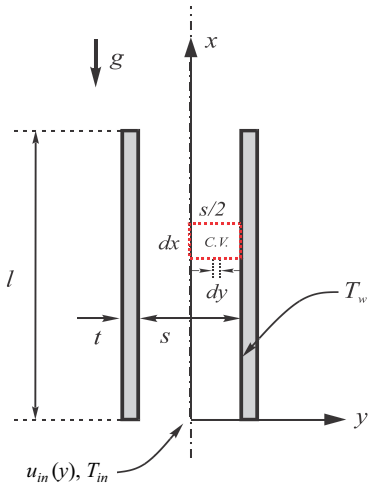

Fig. 3. Schematic of the control volume selected for the channel flow.

$$T_C(x,y) = 4\Delta T e^{-\frac{15\nu x}{s^2 u_{in,C}}}\left(\left(\frac{y}{s}\right)^2 - \frac{1}{4}\right) + T_w \tag{2}$$

The index C is used for the equations related to channel flow to separate them from gap flow parameters, which are indexed by letter G, wherever necessary. The average inlet velocity to each channel, $u_{C,in}$, is used in Eqs. (1) and (2), for sake of simplicity of calculations. This term is required for calculation of the velocity and temperature profiles in each channel. For the first channel located at the bottom row of the fin array, this term can be calculated using Eq. (3), [51] to give;

$$u_{in,C} = \frac{(1-\beta\Delta T)g\beta\Delta T s^2}{12\nu} \tag{3}$$

The term ΔT in Eq. (3) is the difference between wall temperature and average air temperature entering the channel. For the higher rows of channels, the inlet velocity can be calculated using the equations developed for gap region in Section 3. Equations (1) and (2) will be used to find the velocity and temperature profiles in the channels. To calculate the heat transfer from the fins for each channel, using correlations we developed in [51], heat transfer coefficient can be found as;

$$h = \frac{4}{15}\frac{su_{in,C}k}{l\alpha}\left(1 - e^{-\frac{15\alpha l}{s^2 u_{in,C}}}\right) \tag{4}$$

For more details on the channel flow, and the methodology to find the above equations, we encourage the readers to see [51].

3.2. Gap flow

Fig. 4 shows the control volume selected for the gap flow. At steady-state condition, when air leaves a channel with a specific velocity/temperature profile, and since it is not introduced to any external mass, momentum, or heat source, its mass flow, total momentum, and total energy will remain constant. Consequently the flow will go through a one-directional diffusion of mass, momentum, and energy in the direction normal to the velocity of the flow. In other words, as air moves along the x-axis in the gap region, the velocity profile which used to be maximum at the center and minimum on the sides when entering the gap, will start to get flattened, keeping the total momentum of the flow constant. The same phenomenon will happen to the temperature profile, meaning that the temperature profile which had its minimum value at the center and maximum value on the sides when entering the gap, will get more and more flat, maintaining the total energy of the flow.

3.2.1. Governing equations and boundary conditions

Based on the general behavior of the flow, explained above, the assumptions used in this study are listed below;

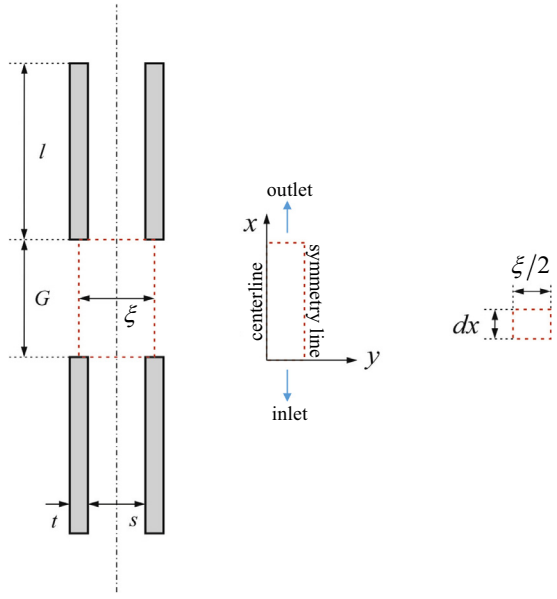

Fig. 4. Schematic of the control volume selected for the gap flow.

- Laminar, steady-state flow.
- 1-Directional flow parallel to the fin walls (velocity component normal to the fin wall is zero).
- 2-Dimensional heat and momentum diffusion in x-direction and y-direction.
- Constant thermo-physical properties.
- No body-force in the gap region.

It is also assumed that the fin height, the depth of domain normal to the paper in Fig. 2, is large enough that the effects of baseplate can be neglected. Applying the assumptions, the momentum and energy conservation equations will be reduced to;

$$u_G\frac{\partial u_G}{\partial x} = \nu\nabla^2 u_G \tag{5}$$

$$u_G\frac{\partial T_G}{\partial x} = \alpha\nabla^2 T_G \tag{6}$$

The conservation equations are subjected to the following boundary conditions;

$$\text{at}\quad y = 0;\qquad \frac{\partial u_G(x,0)}{\partial y} = \frac{\partial T_G(x,0)}{\partial y} = 0 \tag{7}$$

$$\text{at}\quad y = \frac{\xi}{2};\qquad \frac{\partial u_G(x,\frac{\xi}{2})}{\partial y} = \frac{\partial T_G(x,\frac{\xi}{2})}{\partial y} = 0 \tag{8}$$

$$\text{at}\quad x = 0;\qquad u_G(0,y) = u_{in,G}(y),\quad T_G(0,y) = T_{in,G}(y) \tag{9}$$

$$\text{at}\quad x\to\infty;\qquad u_{G,x\to\infty} = \frac{2}{\xi}\int_0^{\frac{\xi}{2}} u_{in,G}(y)dy,$$
$$T_{G,x\to\infty} = \frac{2}{\xi u_{G,x\to\infty}}\int_0^{\frac{\xi}{2}} u_{in,G}(y)T_{in,G}(y)dy \tag{10}$$

Equations (7) and (8) result from geometric symmetry at the gap centerline and at the boundary between two adjacent gaps. The terms u_{in} and T_{in} in Eqs. (9) and (10) are the average gap inlet velocity and temperature respectively. These gap inlet profiles are required to be calculated to be used as inlet boundary condition for each gap. Equation (10) implies that, given enough space to the flow, both the velocity and temperature profiles will reach a uniform state, equal to the bulk momentum and energy entering the gap. Due to the symmetrical boundary condition at x-direction, the uniform velocity and temperature will remain unchanged after reaching this state.

Following Ref. [52] and integrating the conservation equations across the gap in y-direction, from $y = 0$ to $y = \xi/2$ the integral form of governing equations will be obtained as;

$$\frac{\partial}{\partial x}\int_0^{\frac{\xi}{2}} u_G^2 dy = \nu\left[\left(\frac{\partial u_G}{\partial y}\right)_{y=\frac{\xi}{2}} - \left(\frac{\partial u_G}{\partial y}\right)_{y=0}\right] = 0 \tag{11}$$

$$\frac{\partial}{\partial x}\int_0^{\frac{\xi}{2}} u_G T_G dy = \alpha\left[\left(\frac{\partial T_G}{\partial y}\right)_{y=\frac{\xi}{2}} - \left(\frac{\partial T_G}{\partial y}\right)_{y=0}\right] = 0 \tag{12}$$

The interpretation of Eqs. (11) and (12) is that the integral form of momentum and energy does not change along the x-direction, so the governing equations can be re-written as;

$$\int_0^{\frac{\xi}{2}} u_G^2(x,y)dy = \int_0^{\frac{\xi}{2}} u_{in,G}^2(y)dy \tag{13}$$

$$\int_0^{\frac{\xi}{2}} u_G(x,y)T_G(x,y)dy = \int_0^{\frac{\xi}{2}} u_{in,G}(y)T_{in,G}(y)dy \tag{14}$$

Inlet velocity and temperature profiles, $u_{in,G}$ and $T_{in,G}$ are still required to solve Eqs. (13) and (14). They will be found in the following section. To apply the integral technique, knowing the general behavior of the velocity and temperature profiles, we assume a known profile for each. Satisfying conservation laws in a lumped fashion across the region of interest, we can obtain velocity and temperature profiles within acceptable accuracy after applying the boundary conditions.

3.2.2. Integral technique

Considering the symmetrical boundary conditions in y-direction, third order polynomials are assumed for both temperature and velocity profiles;

$$u_G(x,y) = a_1(x)y^3 + b_1(x)y^2 + c_1(x)y + d_1(x) \tag{15}$$

$$T_G(x,y) = a_2(x)y^3 + b_2(x)y^2 + c_2(x)y + d_2(x) \tag{16}$$

Applying the boundary conditions in the y-direction (Eqs. (7) and (8)), into Eqs. (15) and (16), we will have;

$$u_G(x,y) = f_1(x)\left(y^3 - \frac{3\xi}{4}y^2\right) + g_1(x) \tag{17}$$

$$T_G(x,y) = f_2(x)\left(y^3 - \frac{3\xi}{4}y^2\right) + g_2(x) \tag{18}$$

The terms $f_1(x)$, $f_2(x)$, $g_1(x)$ and $g_2(x)$ are all unknown functions that need to be determined, but before applying the governing equations, the terms related to inlet velocity and temperature must be determined. Since Eqs. (17) and (18) are chosen to describe the flow behavior inside the gap region, they should be valid everywhere in the domain, including the entrance. The only difference at the entrance is that the terms $f_1(x)$, $f_2(x)$, $g_1(x)$ and $g_2(x)$ will not be functions of x anymore, and they will be constants. These constants can be found by setting the flow conditions at the channel outlet and gap inlet to be equal.

$$u_{in,G}(0) = u_G(0,0) = u_C(l,0), \quad T_{in,G}(0) = T_G(0,0) = T_C(l,0) \tag{19}$$

$$u_{in,G}\left(\frac{\xi}{2}\right) = u_G\left(0,\frac{\xi}{2}\right) = u_C\left(l,\frac{S}{2}\right) = 0, \quad T_{in,G}\left(\frac{\xi}{2}\right) = T_G\left(0,\frac{\xi}{2}\right) = T_C\left(l,\frac{S}{2}\right) = T_W \tag{20}$$

Applying Eqs. (19) and (20) to Eqs. (19), (20), (17) and (18), the gap inlet velocity and temperature profiles will be obtained as;

$$u_{in,G}(y) = -\frac{1}{v\xi^3}\left(y^3 - \frac{3\xi}{4}y^2 + \frac{\xi^3}{16}\right)\left[(\beta g s^2\Delta T - 8\nu u_{in})e^{-\frac{5\nu l\left(\beta g s^2\Delta T - 24\nu u_{in}\right)}{s^2 u_{in}\left(\beta g s^2\Delta T - 8\nu u_{in}\right)}} - \beta g s^2\Delta T\right] \tag{21}$$

$$T_{in,G}(y) = T_W - \frac{16\Delta T}{\xi^3}\left(y^3 - \frac{3\xi}{4}y^2 + \frac{\xi^3}{16}\right)e^{-\frac{15\nu l}{s^2 u_{in}}} \tag{22}$$

Having the gap inlet velocity and temperature profiles, Eqs. (21) and (22) can be substituted into Eqs. (13) and (14), and then Eqs. (17) and (18) can be substituted into the new governing equations to give;

$$u_G(x,y) = f_1(x)\left(y^3 - \frac{3\xi}{4}y^2 + \frac{\xi^3}{32}\right) - \frac{1}{32v}\left[(\beta g s^2\Delta T - 8\nu u_{in})e^{-\frac{5\nu l\left(\beta g s^2\Delta T - 24\nu u_{in}\right)}{s^2 u_{in}\left(\beta g s^2\Delta T - 8\nu u_{in}\right)}} - \beta g s^2\Delta T\right] \tag{23}$$

$$T_G(x,y) = f_2(x)\left(y^3 - \frac{3\xi}{4}y^2 + \frac{\xi^3}{32} - \frac{17\xi^3}{1120}f_1(x)\right) + T_W - \frac{26\Delta T}{35}e^{-\frac{15\nu l}{s^2 u_{in}}} \tag{24}$$

The conventional way to use the integral method is to apply the two remaining boundary conditions, Eqs. (9) and (10), to Eqs. (23) and (24) to find $f_1(x)$ and $f_2(x)$, but doing so will not help to find the desired parameters. To address this issue, a simplified integral technique is used, and based on the physics of the flow, we assume an exponential behavior for $f_1(x)$ and $f_2(x)$. Physics of the flow and heat transfer suggest that both velocity and temperature at the centerline, will change more rapidly at the beginning of the gap, and approach an asymptotic value as the fluid moves along the x-axis, so;

$$f_1(x) = \phi - \varphi e^{-\varsigma x} \tag{25}$$

$$f_2(x) = \vartheta - \iota e^{-\sigma x} \tag{26}$$

where $\phi, \varphi, \varsigma, \vartheta, \iota$, and σ are constants to be determined. Substituting Eqs. (25) and (26) into Eqs. (23) and (24), and satisfying boundary conditions defined by Eqs. (9) and (10), the temperature and velocity profiles in the gap region will be determined as;

$$u(x,y) = -\frac{1}{32v\xi^3}\left(32y^3e^{-\varsigma x} - 24\xi y^2e^{-\varsigma x} + \xi^3e^{-\varsigma x} + \xi^3\right)\left[(\beta g s^2\Delta T - 8\nu u_{in})e^{-\frac{5\nu l\left(\beta g s^2\Delta T - 24\nu u_{in}\right)}{s^2 u_{in}\left(\beta g s^2\Delta T - 8\nu u_{in}\right)}} - \beta g s^2\Delta T\right] \tag{27}$$

$$T(x,y) = T_w - \left(y^3 - \frac{3\xi}{4}y^2 + \frac{\xi^3}{32} - \frac{17\xi^3}{1120}e^{-\varsigma x}\right)\frac{16\Delta T}{\xi^3}e^{-\frac{15\nu l}{s^2 u_{in}} - \sigma x} - \frac{26\Delta T}{35}e^{-\frac{15\nu l}{s^2 u_{in}}} \tag{28}$$

As can be seen in Eqs. (27) and (28), ς and σ are still unknown, and need to be determined. In order to find the two constants, numerical simulation is used. More details on the numerical simulations is explained in the following section.

4. Numerical simulation

In order to find the unknown constants, ς and σ from the integral solution, a two dimensional numerical model of the gap flow is developed, using the commercially available software package, COMSOL Multiphysics 4.3. Known velocity and temperature profiles are applied to the bottom of domain as inlet condition, and symmetry boundary condition is considered for the sides of the domain. At the top of the domain, outlet pressure is considered to be atmospheric pressure. The numerical domain and the boundary conditions are shown in Fig. 5a.

Different number of mesh elements have been tested and the results were compared for the temperature in the outlet at the centerline, to ensure a mesh independent solution. Accordingly, choosing a mesh number of 1000, we found a 0.05% deviation in the results, compared to the simulation of the gap with mesh number of 100. Similarly, the results for simulation with 2000 mesh elements deviated up to 0.01%, compared to those from the case with 1000 elements. Therefore, we chose element number of 1000 for numerical investigation purposes. Fig. 6 shows the grid independency analysis for the benchmark case. As can be observed in the figure, the number of elements does not have significant effect on the results, and the simulation is not very sensitive to the grid size. Table 1 lists the parameters used for the benchmark case. Fig. 5b shows a sample of the grid used in numerical studies. Velocity distribution, and temperature distribution obtained from numerical simulation on the benchmark case are shown in Fig. 5c and d, respectively.

Comparing the results from integral technique and the numerical simulation results and trying to fit the temperature and velocity profiles, the unknown constants, ς and σ for air, will be found as follow;

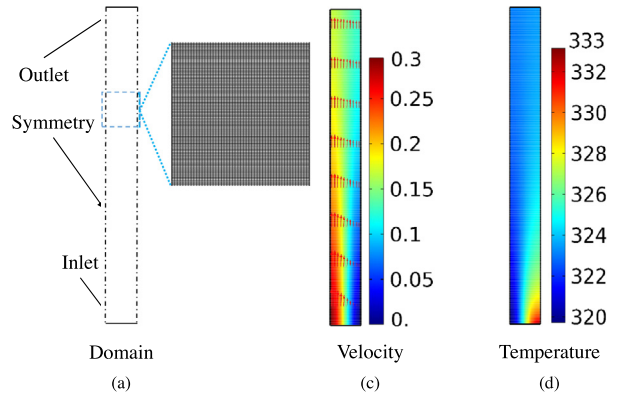

Fig. 5. Numerical simulation-benchmark case; (a) the domain and boundary condition, (b) a sample of mesh, (c) velocity distribution, and (d) temperature distribution.

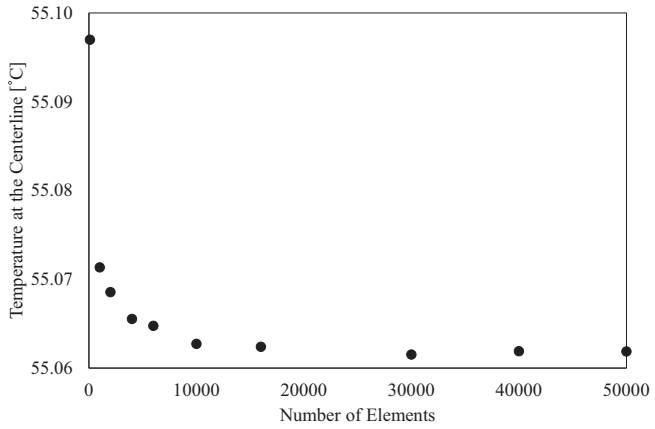

Fig. 6. Mesh independency study for the benchmark case.

$$\varsigma = 40 \tag{29}$$

$$\sigma = 95 \tag{30}$$

Substituting the obtained constants in the gap velocity and temperature profiles, Eqs. (27) and (28), closed-form solution are obtained for temperature and velocity inside the gap. Fig. 7 shows the worst case we observed, comparing the results from integral solution and numerical simulation with the constants introduced in Eqs. (29) and (30). The maximum relative difference between the integral solution and numerical simulation, is 5.4% and 8.6%, respectively for velocity and temperature distribution.

5. Experimental study

The objective of the experimental study is to verify the results of the method proposed for calculating total heat transfer from the interrupted fins in Section 6.1. To accomplish this, a custom-made testbed was designed and built, and 13 finned plate samples, with different fin spacing, gap length, and fin length were prepared. A series of tests with different average surface temperatures were conducted to validate the results from integral solution.

5.1. Testbed

A custom-made testbed is designed for measuring natural convection heat transfer from the finned heatsinks, as shown in Fig. 8.

Table 1
Parameters used for numerical simulation benchmark case.

Parameter	Description	Value	Unit
G	Gap length	5	[cm]
ξ	Gap width	11	[mm]
$u_{in,max}$	Maximum velocity at the inlet temperature (centerline)	0.3	[m/s]
$u_{in,min}$	Minimum velocity at the inlet (side boundaries)	0	[m/s]
$T_{in,max}$	Maximum temperature at the inlet (side boundaries)	60	[°C]
$T_{in,min}$	Minimum temperature at the inlet temperature (centerline)	47	[°C]

The set-up includes a wooden frame which is insulated at the backside by two layers of compressed polyester foam with a thickness of 25 mm each. The input heat is provided by a 30 cm long 150 W Chromalox strip heater, attached to the backside of the sample. High conductive thermal paste provided by Omega is used to minimize the thermal contact resistance between the heater and the samples. A variable voltage regulator, Variac model SC-20M, is used to provide the power to the heater. To measure the temperature, *T*-type thermocouples provided by Omega, are attached to backside of the samples. Data logging is performed through a data acquisition system (DAQ), supplied by National Instrument. The supplied AC voltage and current to the heater are measured by National Instruments DAQ modules, NI 9225 and NI 9227, respectively. Temperature data are logged by National Instruments DAQ module, NI 9213.

Thirteen samples with the same fin height and baseplate dimensions are prepared. To ensure similar surface finishing for all the samples, CNC machining was used to prepare the samples. Geometrical dimensions of the samples are designed in a way to enable parametric study on fin spacing, fin length, and gap length. Based on the developed model, fin parameters are selected to cover the optimum range. Dimensions of the test samples are given in Table 2.

5.2. Test procedure

The experiments are performed in a windowless room with an environment free of air currents. The room dimensions are selected to be large enough to ensure constant ambient temperature during the test. The input power supplied to the heaters is monitored and surface temperatures were measured at five locations at the back of the baseplate. Four self-adhesive, copper-constantan thermocouples (Omega, *T*-type) are attached in vertical locations on one side of the samples backplate, as shown in Fig. 8a. An extra thermocouple is installed on the same level with the lowest thermocouples, at the other side of backplate, to make sure that the temperature is well distributed horizontally (T_5 in Fig. 8a). All thermocouples are taped down to the backside of the samples to prevent disturbing the air flow on the finned side of the samples. An additional thermocouple is used to measure the ambient temperature during the experiments. Temperature measurements are performed at five points and the average value is taken as the baseplate temperature. Among all the experiments, the maximum standard deviation from the average temperature is measured to be less than 2.5 °C. Since the experiments are performed to mimic the uniform wall temperature boundary condition, the thickness of the baseplate and the fins are selected fairly high, 5 mm and 3 mm, respectively, to ensure the minimum thermal bulk resistance and uniform temperature distribution in the samples. An infrared camera, model SC655 from FLIR, is used to observe the temperature variation along the fins. The maximum temperature difference between the fins and the baseplate

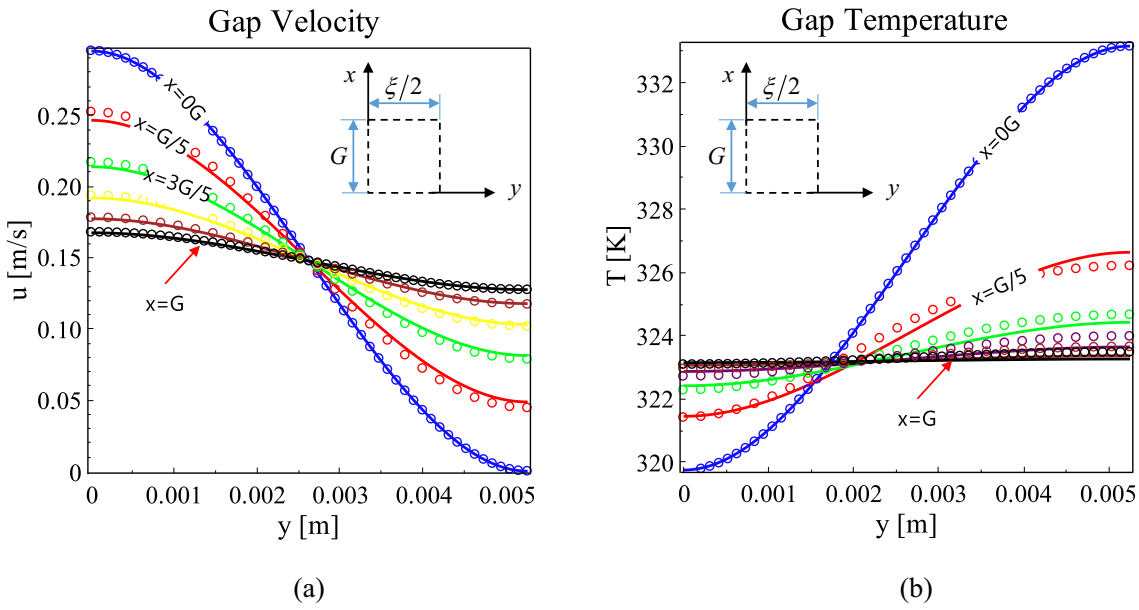

Fig. 7. Comparison between the result from integral technique with $\varsigma = 40$ and $\sigma = 95$ and numerical simulations at the benchmark case, (a) velocity domain, (b) temperature domain.

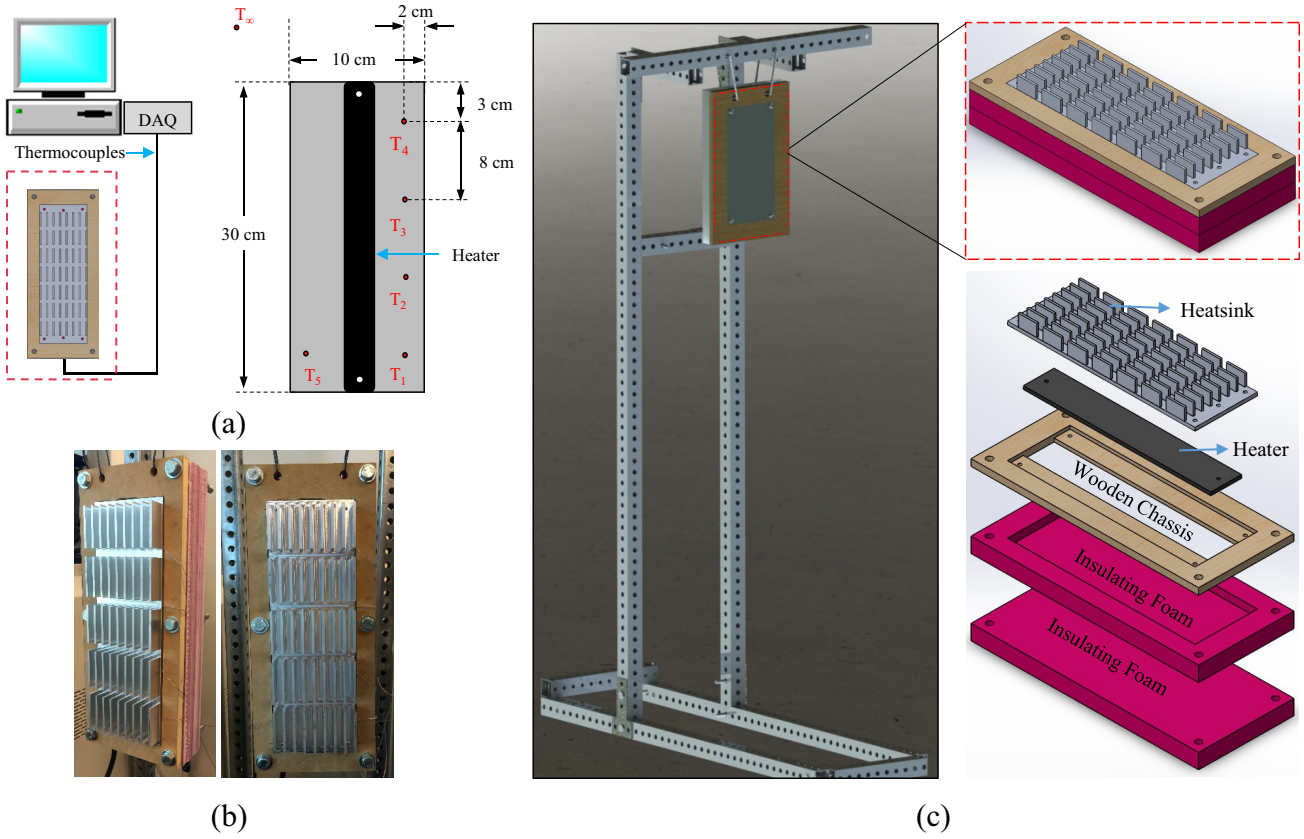

Fig. 8. Experimental setup, (a) the position of thermocouples and the heater, (b) photos of sample under test, (c) schematic of the test bed and insulations.

is measured to be about 2.1 °C, so the fins are assumed to be at the same temperature with the baseplate. For each of the 13 samples, the experimental procedure is repeated for different power inputs. Table 3 lists the range of some important test parameters. The steady-state condition is considered to be achieved when the rate of all temperature variations are less than 0.1 °C/hr which in average, takes 120 min for the test samples used in the experiments.

Table 2
Dimensions of the interrupted fin samples used in the experiments.

Schematic and sample photos	Sample name	s [mm]	l [mm]	G [mm]	m	n
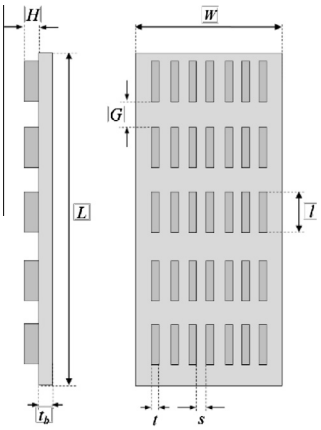	Int. 9-30-10	9	30	10	7	9
	Int. 9-10-10	9	10	10	15	9
	Int. 9-20-10	9	20	10	10	9
	Int. 9-40-10	9	40	10	6	9
	Int. 9-50-10	9	50	10	5	9
	Int. 9-140-10	9	140	10	2	9
	Int. 5-30-10	5	30	10	7	13
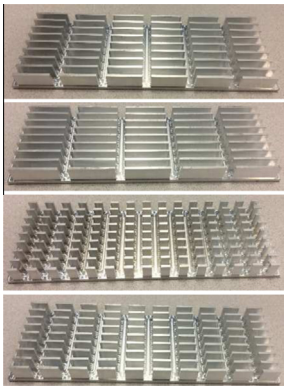	Int. 7-30-10	7	30	10	7	10
	Int. 11-30-10	11	30	10	7	8
	Int. 13-30-10	13	30	10	7	7
	Int. 9-30-6	9	30	6	1	9
	Int. 9-30-8	9	30	8	8	9
	Int. 9-300-0	9	300	0	8	9

Table 3
Range of some important parameters in test procedure.

Parameter	Description	Range	Unit
P	Heater power	5–50	[W]
T_∞	Ambient temperature	24–27	[°C]
T_W	Wall temperature	30–70	[°C]

For the data analysis, heat transfer due to natural convection from the baseplate and fin tips are calculated using the available correlations in literature [15], and subtracted from total heat input to the system. Following Rao et al. [53], the effect of radiation heat transfer is also subtracted from the fins total heat transfer. Due to relatively low surface temperature and low emissivity of machined aluminum (between 0.09 and 0.1 [54]), the effect of radiation is not significant. The maximum calculated value for radiation heat transfer is 3.2% of total heat transfer.

5.3. Uncertainty analysis

Voltage (V) and current (I) are the electrical parameters measured in our experiments, from which the input power, P_{input}, can be calculated. The total accuracy in the measurements is evaluated based on the accuracy of the employed instruments. The maximum uncertainty for the measurements can be obtained using the uncertainty concept provided in [55]. To calculate the uncertainty with the experimental measurements the following relation is used [55]:

$$\omega_R = \left[\sum \left(\frac{\partial R}{\partial x_i}\omega_i\right)^2\right]^{\frac{1}{2}} \tag{31}$$

where ω_R is the uncertainty in results, $R(x_1, x_2, \ldots, x_n)$, and ω_i is the uncertainty of the independent variable x_i. The final form of the uncertainty for the input power becomes;

$$P_{input}[W] = V.I \tag{32}$$

$$\frac{\delta P_{input}}{P_{input}} = \left[\left(\frac{\delta V}{V}\right)^2 + \left(\frac{\delta I}{I}\right)^2\right]^{\frac{1}{2}} \tag{33}$$

$$\frac{\delta \dot{Q}_{Rad.}}{\dot{Q}_{Rad.}} = \left[4\left(\frac{\delta T_w}{T_w}\right)^2 + 4\left(\frac{\delta T_\infty}{T_\infty}\right)^2 + \left(\frac{\delta L}{L}\right)^2 + \left(\frac{\delta W}{W}\right)^2 + \left(\frac{\delta t}{t}\right)^2\right]^{\frac{1}{2}} \tag{34}$$

$$\dot{Q}_{N.C.}[W] = P_{input} - \dot{Q}_{Rad.} \tag{35}$$

Substituting the values for $V, I, T_w, T_\infty, L, W$, and t, into Eqs. (34) and (35), the maximum uncertainty value for natural convective heat transfer, $\dot{Q}_{N.C.}$ is calculated to be 8%. The temperatures uncertainty ΔT is 2 °C which is twice as the accuracy of the T-type thermocouples i.e. ±2 °C. The calculated uncertainties reported as error bars in the experimental results.

5.4. Test results

The comparison between the experimental data and the values obtained from the combination of the channel solution and gap solution are shown in Fig. 9 for different values of ΔT, which is the difference between average surface temperature and ambient temperature. The details on how to calculate the total heat

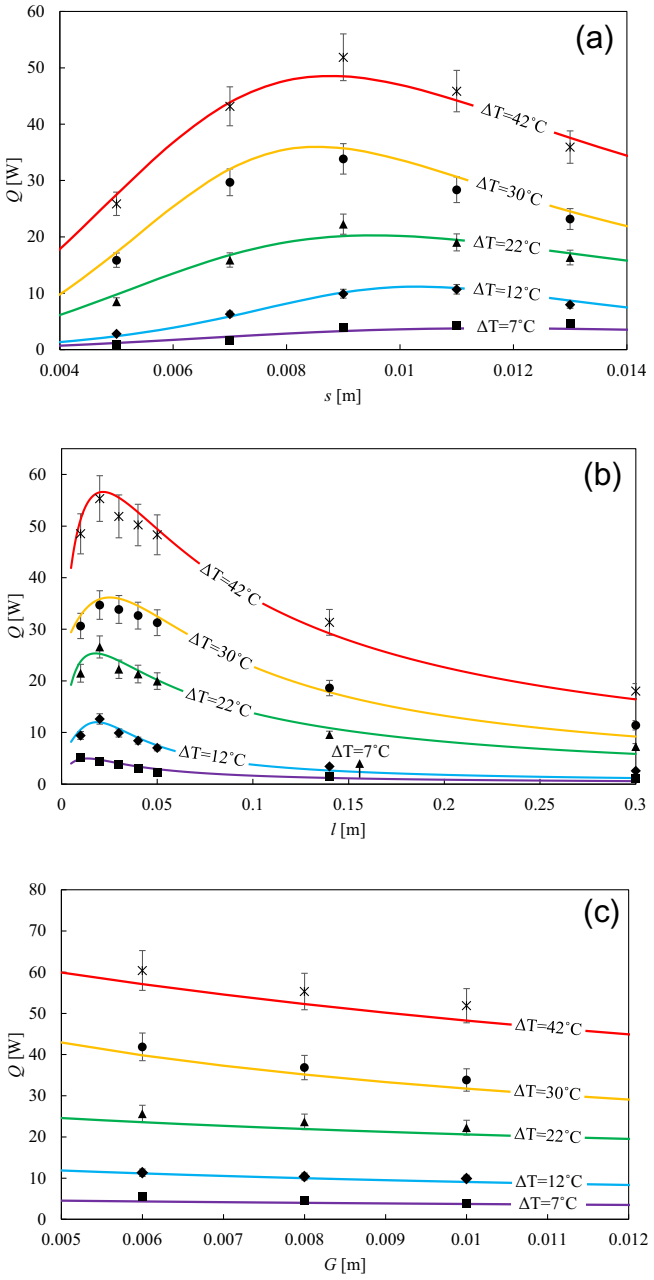

Fig. 9. Comparison between the experimental data and analytical solution, (a) fin spacing, (b) fin length, (c) gap length.

transfer to develop the analytical results of Fig. 9 are explained in Section 6.1. As can be seen in the figure, there is a fairly good agreement between the experimental data and the analytical solution. For the fin spacing, s, the maximum, minimum, and average relative difference between the experimental data and closed-form solution is 32%, 2% and 10%, respectively (Fig. 9a). These values for the fin length, l, are 26%, 1% and 11%, respectively (Fig. 9b). Comparing the result from analytical solution to the experimental data, gives maximum, minimum, and average relative difference of 23%, 1% and 7%, respectively for the gap length, G (Fig. 9c). Maximum errors always occur at low temperature differences between the surface and ambient, $\Delta T \approx 7\ ^{\circ}C$, which is not normally a value for naturally-cooled heatsinks in real applications.

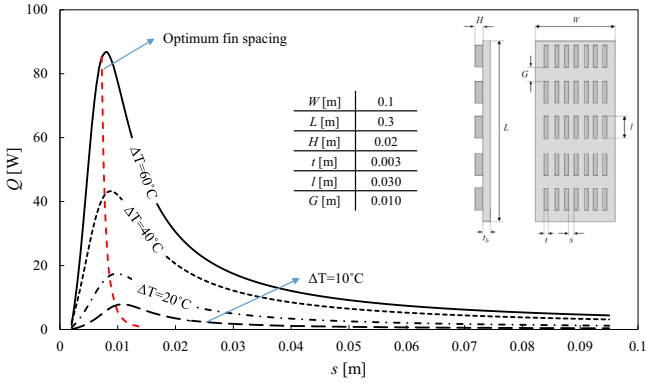

Fig. 10. Effect of fin spacing on heat transfer from the heatsink.

6. Results and discussions

6.1. Heat transfer calculation procedure

Having geometrical parameters, fin height, H, fin thickness, t, fin spacing, s, fin length, l, and gap length, G, known, on a baseplate with dimensions, L and W, number of fin rows, m, and number of fin columns, n, can be calculated as follows;

$$m = \frac{L}{l+G} \tag{36}$$

$$n = \frac{W}{s+t} \tag{37}$$

The total heat transfer area can be calculated as follows;

$$A = 2mnlH \tag{38}$$

To calculate the heat flux from the first row of fins, Eq. (3) for the inlet velocity to the first row, $u_{C,in,1}$, can be substituted into Eq. (4) to find the heat transfer coefficient associated with first row of fins, h_1. The calculated heat transfer coefficient can be substituted in Eq. (39) to find the heat flux, knowing that the inlet temperature to the first row, $T_{C,in,1}$, is equal to ambient temperature, T_∞.

$$q_1 = h_1(T_w - T_{in,C,1}) \tag{39}$$

Now Eqs. (21) and (22) can be used to find the inlet condition to the first gap $u_{G,in,1}$ and $T_{G,in,1}$. Having the first gap inlet conditions, Eqs. (23) and (24) can be used to calculate the average inlet velocity $(u_{C,in,2})$ and temperature $(T_{C,in,2})$ to the second row of fins. The same procedure can be followed to find the heat flux for the ith row of fins, until the March through all the rows is finished. The total heat flux and total heat transfer can be found as follows;

$$q = \sum_{i=1}^{m} q_i \tag{40}$$

$$Q = Aq \tag{41}$$

All fluid properties can be evaluated at the average temperature, $T_{avg} = (T_w + T_\infty)/2$. A simple computer code, in any language, can be developed to find the heat flux and total heat transfer from any arbitrary fin arrangement.

6.2. Parametric study

6.2.1. Effect of fin spacing

Fig. 10 shows the effect of fin spacing on total heat transfer from the heatsink. As expected, an optimum fin spacing exists that

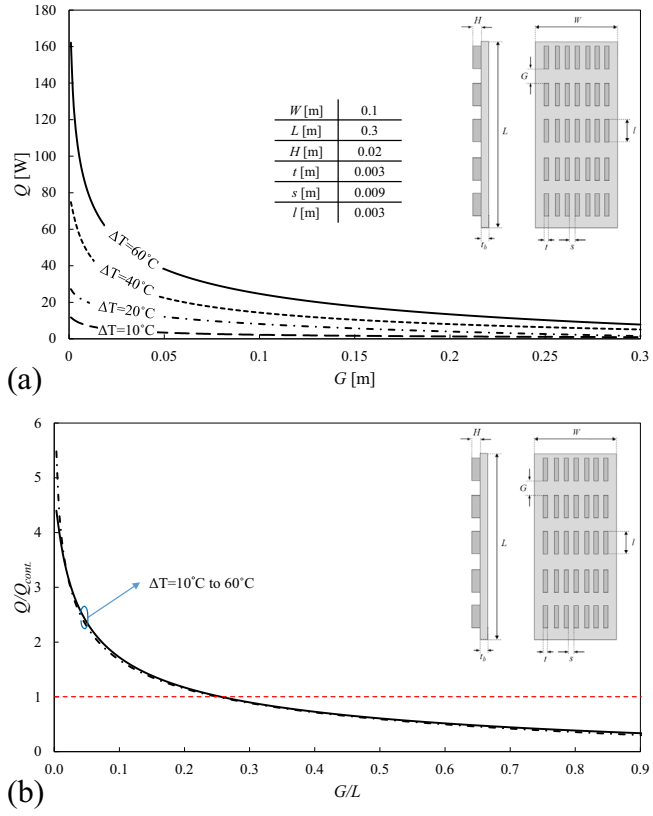

Fig. 11. Effect of gap length on heat transfer from the heatsink, (a) total heat transfer, (b) dimensionless heat transfer with respect to continuous fins.

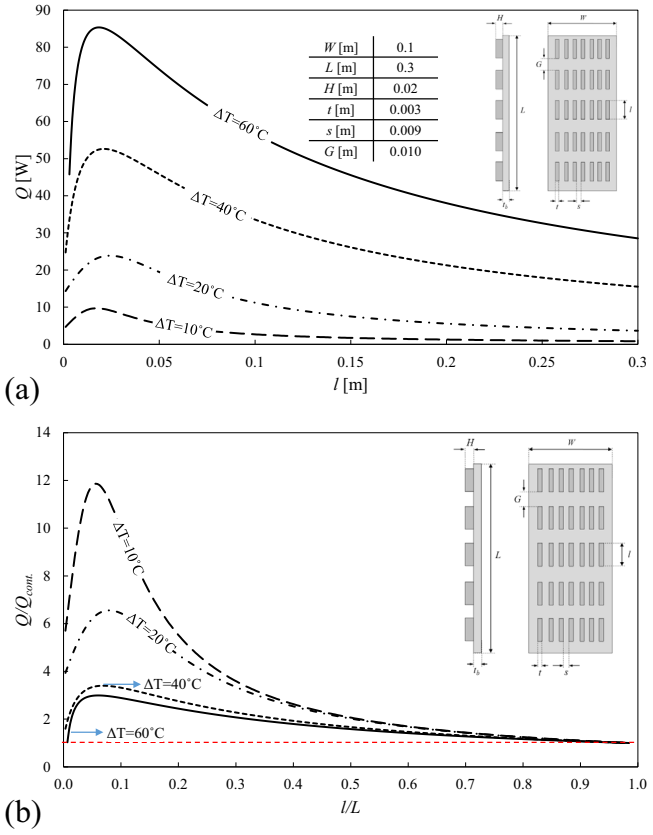

Fig. 12. Effect of fin length on heat transfer from the heatsink, (a) total heat transfer, (b) dimensionless heat transfer with respect to continuous fins.

maximizes the heat transfer and interestingly enough, our various parametric studies show that the optimum fin spacing will remain unchanged compared to continuous fins case. Therefore, the correlation from [22] for optimum fin spacing is valid for case of interrupted fins as well.

$$s_{opt.} = 2.714\left[\frac{\nu\alpha L}{g\beta(T_w - T_\infty)}\right]^{\frac{1}{4}} \tag{42}$$

6.2.2. Effect of gap length

The effect of gap length on total heat transfer at different temperatures is shown in Fig. 11a. At first look, one may conclude that the best gap length is $G = 0$; however, it should be noted that gap length has an asymptotic effect on the heat transfer. As $G \to 0$, total heat transfer will increase dramatically but at $G = 0$, which is related to continuous fins, there will be a sudden drop in total heat transfer value. To shed more light on the effect of gap length, Fig. 11b shows the ratio of heat transfer from interrupted fins to the heat transfer from continuous fins with the same fin spacing, $Q/Q_{cont.}$, versus G/L. This figure shows how at small values of gap length the heat transfer from interrupted fins dominate the heat transfer from continuous fins, due to the effect of gap on thermal boundary layer. As the gap length increases, due to loss of heat transfer area, total heat transfer keeps decreasing until the interrupted fin arrangement loses its privilege over continuous fins. It is also worth mentioning that as gap length increases, the weight of heatsink decreases, which can play a key role for the applications in which weight is an important matter.

6.2.3. Effect of fin length

Fig. 12a shows the total heat transfer from the fins for different fin lengths at various surface temperatures. As shown in the figure, fin length plays an important role in the heatsink performance. Depending on the baseplate dimensions, an optimum fin length can be found to maximize the total heat transfer rate. Fig. 12b shows the ratio of heat transfer from interrupted fins to continuous fins, which as shown, can be over 12 times more for the specific case shown in Fig. 12b.

A noteworthy trend that can be observed in Fig. 12b is that the enhancement effect of adding interruptions to the fins decreases at higher temperatures. The reason for this phenomena is that the buoyancy force is stronger at higher temperatures, causing more air flow to pass from the channel. More air flow leads to higher velocity and heat transfer rate. Adding interruption to fins at high surface temperatures, decreases this effect by removing high temperature solid surface, which is the main cause for buoyancy force. However at practical ranges of heatsink temperature, $40 - 60\ ^\circ C$, interrupted fin arrangement can dissipate heat about 3 times more than continuous fins, which is still a considerable contribution to the heatsink performance.

6.3. Heatsink design procedure

In this section, it is intended to find the best fin arrangement, by determining the geometrical parameters, to maximize the total heat transfer rate from an available surface area, with a known operating temperature. The design procedure for the fin arrangement is explained in this section as following;

Step 1: Selecting the fin thickness, t. Fin thickness selection is mostly a matter of mechanical strength, so depending on the application and required robustness of the heatsink, the fin thickness can be selected. However, when selecting

the thickness of the fins, we should keep in mind that thicker fins present lower thermal bulk resistance, which leads to more uniform temperature distribution along the fin and higher heat transfer. It also worth noting that thicker fin means heavier heatsink.

Step 2: Calculating the optimum fin spacing, $s_{opt.}$, using Eq. (42). The number of fin columns can be evaluated using Eq. (37), when the optimum fin spacing is determined.

Step 3: Determining the gap length, G. Selecting the gap length is highly dependent on manufacturing limitations, cost, and weight considerations. As shown in Section 6.2, the smaller gap length leads to higher total heat transfer rate; however sometimes due to manufacturing limitations, small gap length is not practical. Very small gaps can also get blocked due to contamination and corrosion and lose their effects. On the other hand, the higher the gap, the lighter the heatsink. Therefore, in applications where weight is a limiting factor, higher gap lengths are better choices. Based on the above-mentioned considerations, one or more gap length option(s) can be selected for the analysis in next step.

Step 4: Finding the optimum fin length. Having all the fin parameters determined, and assuming an average operation temperature for the heatsink, a simple computer code can be used to perform a parametric study on the fin length to maximize the total heat transfer from the heatsink.

7. Conclusion

A new analytical solution for steady-state laminar natural convection from isothermal vertical rectangular interrupted fins is presented and close-form compact correlations are introduced for velocity and temperature distribution for the first time. Integral technique was used in combination with numerical simulations to solve the governing equation. A custom-made testbed is built and 13 different aluminum heatsinks are tested to validate the numerical and analytical results. An easy-to-apply method is introduced, using the obtained correlations, to calculate total heat transfer from any arbitrary arrangement of interrupted fins, and a step-by-step method is presented to design naturally-cooled heatsinks with interrupted fins. Results show that naturally-cooled heatsinks with interrupted fins are capable of dissipating heat up to 12 time higher than currently available heatsinks with similar baseplate dimensions. This is while the weight of such heatsinks can get up to 30% lighter than the heatsinks with continuous fins, but similar baseplate dimensions.

References

[1] S. Anandan, V. Ramalingam, Thermal management of electronics: a review of literature, Int. J. Therm. Sci. 12 (2) (2008) 5–26.

[2] S.P.S. Gurrum, S. Suman, K. Shivesh, Y.K. Joshi, A.G. Fedorov, Thermal issues in next-generation integrated circuits, IEEE Trans. Device Mater. Reliab. 4 (4) (2004) 709–714.

[3] BCCResearch, 2014, The Market for Thermal Management Technologies, Wellesley, MA, USA.

[4] D.C. Kilper, S. Member, G. Atkinson, S.K. Korotky, S. Goyal, P. Vetter, D. Suvakovic, O. Blume, Power trends in communication networks, Sel. Top. Quantum Electron. 17 (2) (2011) 275–284.

[5] C. Lubritto, A. Petraglia, Telecommunication power systems: energy saving, renewable sources and environmental monitoring, in: IEEE Electrical Power & Energy Conference (EPEC), Vancouver Canada, 2008, pp. 1–4.

[6] D. Hernon, P. Silvestre-Castillo, P. Hayden, Significantly extending the operational range of free cooling in radio base station indoor shelters, in: IEEE 33rd International Telecommunications Energy Conference (INTELEC), IEEE, Amsterdam, Netherlands, 2011, pp. 1–7.

[7] M. Ahmadi, G. Mostafavi, M. Bahrami, Natural convection from rectangular interrupted fins, Int. J. Therm. Sci. 82 (1) (2014) 62–71.

[8] M. Fujii, Enhancement of natural convection heat transfer from a vertical heated plate using inclined fins, Heat Transfer Res. 36 (6) (2007) 334–344.

[9] A. Daloglu, T. Ayhan, Natural convection in a periodically finned vertical channel, Int. Commun. Heat Mass Transfer 26 (8) (1999) 1175–1182.

[10] S.A. Nada, Natural convection heat transfer in horizontal and vertical closed narrow enclosures with heated rectangular finned base plate, Int. J. Heat Mass Transfer 50 (3–4) (2007) 667–679.

[11] A. Ben-Nakhi, A.J. Chamkha, Conjugate natural convection in a square enclosure with inclined thin fin of arbitrary length, Int. J. Therm. Sci. 46 (5) (2007) 467–478.

[12] S. Ostrach, An analysis of laminar free-convection flow and heat transfer about a flat plate parallel to the direction of the generating body force, 1952.

[13] E. Sparrow, J. Gregg, Laminar free convection from a vertical plate with uniform surface heat flux, ASME J. Heat Transfer 78 (1) (1956) 435–440.

[14] J. Merkin, A note on the similarity solutions for free convection on a vertical plate, J. Eng. Math. 19 (1) (1985) 189–201.

[15] S.W. Churchill, H. Chu, Correlating equations for laminar and turbulent free convection from a vertical plate, Int. J. Heat Mass Transfer 18 (11) (1975) 1323–1329.

[16] M. Yovanovich, K. Jafarpur, Bounds on laminar natural convection from isothermal disks and finite plates of arbitrary shape for all orientations and Prandtl numbers, in: ASME Winter Annual Meeting, New Orleans, Louisiana, 1993, pp. 93–111.

[17] R. Cai, N. Zhang, Explicit analytical solutions of 2-D laminar natural convection, Int. J. Heat Mass Transfer 46 (5) (2003) 931–934.

[18] T. Yousefi, M. Ashjaee, Experimental study of natural convection heat transfer from vertical array of isothermal horizontal elliptic cylinders, Exp. Therm. Fluid Sci. 32 (1) (2007) 240–248.

[19] S. Suryawanshi, N. Sane, Natural convection heat transfer from horizontal rectangular inverted notched fin arrays, J. Heat Transfer 131 (8) (2009) 797–805.

[20] W. Elenbaas, Heat dissipation of parallel plates by free convection, Physica 9 (1) (1942) 1–28.

[21] Stuart W. Churchill, A comprehensive correlation equation for buoyancy induced flow in channels, Lett. Heat Mass Transfer 4 (3) (1977) 193–199.

[22] A. Bar-Cohen, W.M. Rohsenow, Thermally optimum spacing of vertical, natural convection cooled, parallel plates, J. Heat Transfer 106 (1) (1984) 116–123.

[23] J.R. Bodoia, J.F. Osterle, The development of free convection between heated vertical plates, J. Heat Transfer 84 (1) (1962) 40–44.

[24] O. Ofi, H.J. Hetherington, Application of the finite element method to natural convection heat transfer from the open vertical channel, Int. J. Heat Mass Transfer 20 (11) (1977) 1195–1204.

[25] J.R. Culham, M.M. Yovanovich, S. Lee, Thermal modeling of isothermal cuboids and rectangular heat sinks cooled by natural convection, IEEE Trans. Compon. Packag. Manuf. Technol. A 18 (3) (1995) 559–566.

[26] E.M. Sparrow, S. Acharya, A natural convection fin with a solution-determined nonmonotonically varying heat transfer coefficient, J. Heat Transfer 103 (2) (1981) 218–226.

[27] K.E. Starner, H.N. McManus, An experimental investigation of free-convection heat transfer from rectangular-fin arrays, J. Heat Transfer 85 (3) (1963) 273–275.

[28] J.R. Welling, C.B. Wooldridge, Free convection heat transfer coefficients from rectangular vertical fins, J. Heat Transfer 87 (4) (1965) 439.

[29] J. Edwards, J. Chaddock, An experimental investigation of the radiation and free convection heat transfer from a cylindrical disk extended surface, ASHRAE Trans. 69 (1) (1963) 313–322.

[30] J. Chaddock, Natural convection heat transfer from vertical rectangular fin array, ASHRAE J 12 (August) (1970) 53–60.

[31] T. Aihara, Natural convection heat transfer from vertical rectangular fin arrays: (Part 3, heat transfer from fin flats), Trans. Jpn. Soc. Mech. Eng. 13 (64) (1970) 1192–1200.

[32] T. Aihara, Natural convection heat transfer from vertical rectangular fin arrays: (Part 2, heat transfer from fin edges), Trans. Jpn. Soc. Mech. Eng. 36 (282) (1970) 239–247.

[33] T. Aihara, Natural convection heat transfer from vertical rectangular fin arrays: (Part 1, heat transfer from base plates), Trans. Jpn. Soc. Mech. Eng. 36 (261) (1970) 915–926.

[34] T. Aihara, Natural convection heat transfer from vertical rectangular-fin arrays: Part 4, Heat-transfer characteristics of nonisothermal-fin arrays, Trans. Jpn. Soc. Mech. Eng. 36 (292) (1970) 2077–2086.

[35] C.W. Leung, S.D. Probert, Heat exchanger: optimal separation for vertical ractangualr fins proturding from vertical rectangular base, Appl. Energy 19 (1) (1985) 77–85.

[36] C.W. Leung, S.D. Probert, M.J. Shilston, Heat exchanger design: optimal uniform separation between rectangular fins protruding from a vertical rectangular base, Appl. Energy 19 (4) (1985) 287–299.

[37] C. Leung, S. Probert, M. Shilston, Heat exchanger design: thermal performances of rectangular fins protruding from vertical or horizontal rectangular bases, Appl. Energy 20 (2) (1985) 123–140.

[38] C. Leung, S. Probert, M. Shilston, Heat transfer performances of vertical rectangular fins protruding from rectangular bases: effect of fin length, Appl. Energy 22 (4) (1986) 313–318.

[39] C.W. Leung, S.D. Probert, Natural-convective heat exchanger with vertical rectangular fins and base: design criteria, Proc. Inst. Mech. Eng. C J. Mech. Eng. Sci. 201 (5) (1987) 365–372.

[40] C.W. Leung, S.D. Probert, Heat-exchanger performance: effect of orientation, Appl. Energy 33 (4) (1989) 235–252.

[41] C.W. Leung, S.D. Probert, Thermal effectiveness of short-protrusion rectangular heat exchanger fins, J. Appl. Energy 34 (1) (1989) 1–8.
[42] D. Van de Pol, J. Tierney, Free convection heat transfer from vertical fin-arrays, IEEE Parts Hybrids Packag. 10 (4) (1974) 267–271.
[43] N.C. Dejong, A.M. Jacobi, An Experimental Study of Flow and Heat Transfer in Offset Strip and Louvered-Fin Heat Exchangers, Urbana, 1995.
[44] J.M. Brutz, J.C. Dutton, A.M. Jacobi, Use of Unsteady Forcing in Interrupted-Fin Heat Exchangers: An Assessment of Potential, Urbana, 2005.
[45] S. Ndao, Y. Peles, M.K. Jensen, Multi-objective thermal design optimization and comparative analysis of electronics cooling technologies, Int. J. Heat Mass Transfer 52 (19–20) (2009) 4317–4326.
[46] A.K.K. Da Silva, S. Lorente, A. Bejan, Optimal distribution of discrete heat sources on a wall with natural convection, Int. J. Heat Mass Transfer 47 (2) (2004) 203–214.
[47] N. Sobel, F. Landis, W. Mueller, Natural convection heat transfer in short vertical channels including effects of stagger, in: Proceedings of 3rd International Heat Transfer Conference, 2(1), pp. 121–125.
[48] E.M. Sparrow, C. Prakash, Enhancement of natural convection heat transfer by a staggered array of discrete vertical plates, J. Heat Transfer 102 (2) (1980) 215–220.
[49] V. Gorobets, Heat transfer for vertical surfaces with discrete fins in the case of free convection, J. Eng. Phys. Thermophys. 75 (5) (2002) 100–107.
[50] G. Mostafavi, Natural convective heat transfer from interrupted rectangular fins (M.A.Sc. Thesis), School of Mechatronic Systems Engineering, Simon Fraser University, 2012.
[51] M. Ahmadi, M. Fakoor-Pakdaman, M. Bahrami, Natural convection from vertical parallel plates: an integral method solution, J. Thermophys. Heat Transfer (2014) 1–10.
[52] A. Bejan, Convection Heat Transfer, John Wiley and Sons Inc, New York, 2004.
[53] V.D. Rao, S.V. Naidu, B.G. Rao, K.V. Sharma, Heat transfer from a horizontal fin array by natural convection and radiation—a conjugate analysis, Int. J. Heat Mass Transfer 49 (19–20) (2006) 3379–3391.
[54] J.P. Holman, Heat Transfer, McGrawHill, Boston, 2010.
[55] J.P. Holman, Experimental Methods for Engineers, McGrawHill, New York, 2001.